2001-FD-ABS-051

MATRIX VISCOSITY AND PRECONDITIONING FOR ROTATING TURBOMACHINERY

M. L. Celestina
A.P. Solutions, Inc.
Cleveland, OH 44135
mark.celestina@grc.nasa.gov

E. Turkel
School of Mathematical Sciences
Sackler Faculty of Exact Sciences
Tel-Aviv University, Tel-Aviv, Israel
turkel@math.tau.ac.il

INTRODUCTION

We consider the solution of the steady state compressible Navier-Stokes equations for both stationary and rotating turbomachinery. This is augmented by a $k - \varepsilon$ turbulence model. The body boundary is modeled using wall functions which allows the use of grids of moderate large aspect ratios. To account for the effect of rotation, we introduce a rotating frame of reference. To simplify the boundary conditions we use the absolute velocity components as the dependent variables. We use a generalized coordinate system starting from cylindrical coordinates.

We solve these equations by marching the time dependent equations in pseudo-time. A Runge-Kutta scheme is used with local time-stepping and residual smoothing. The space differencing is a central difference finite volume scheme with an artificial viscosity. The artificial viscosity contains a second difference portion to prevent overshoots near shocks. This is turned off in smooth regions of the flow. The fourth difference viscosity is designed to reduce the high wave number components of the error. To prevent overshoots, this part is turned off near shocks. This dissipation algorithm of Jameson, Schmidt and Turkel [3] is based on a scalar coefficient, proportional to the largest eigenvalue of the Jacobian matrix in each direction. This has been improved by the addition of both a matrix valued coefficient in the artificial viscosity [7] and low speed preconditioning [8; 9; 12]. The preconditioning improves both the rate of convergence to a steady state and also the accuracy for low Mach number flows. Both the matrix viscosity and the preconditioning techniques are based on the inviscid equations even though the results use the Navier-Stokes equations [13]. Some early results for turbomachinery using preconditioning were presented in [14].

EQUATIONS

The Euler equations in cylindrical coordinates are given by

$$\frac{\partial(r\rho)}{\partial t} + \frac{\partial(r\rho v_r)}{\partial r} + \frac{\partial(\rho v_\theta)}{\partial \theta} + \frac{\partial(r\rho v_z)}{\partial z} = 0$$

$$\frac{\partial(r\rho v_r)}{\partial t} + \frac{\partial(r(\rho v_r^2 + p))}{\partial r} + \frac{\partial(\rho v_r v_\theta)}{\partial \theta} + \frac{\partial(r\rho v_r v_z)}{\partial z} = \rho v_\theta^2 + p$$

$$\frac{\partial(r^2\rho v_\theta)}{\partial t} + \frac{\partial(r^2\rho v_\theta v_r)}{\partial r} + \frac{\partial(r(\rho v_\theta^2 + p))}{\partial \theta} + \frac{\partial(r^2\rho v_\theta v_z)}{\partial z} = 0$$

$$\frac{\partial(r\rho v_z)}{\partial t} + \frac{\partial(r\rho v_r v_z)}{\partial r} + \frac{\partial(\rho v_\theta v_z)}{\partial \theta} + \frac{\partial(r(\rho v_z^2 + p))}{\partial z} = 0$$

$$\frac{\partial(r\rho E)}{\partial t} + \frac{\partial(r\rho H v_r)}{\partial r} + \frac{\partial(\rho H v_\theta)}{\partial \theta} + \frac{\partial(r\rho H v_z)}{\partial z} = 0$$

where the total internal energy, E, and the total enthalpy, H, are

$$E = \frac{p}{(\gamma - 1)\rho} + \frac{1}{2}\left(v_r^2 + v_\theta^2 + v_z^2\right) \quad H = E + \frac{p}{\rho} \quad (1)$$

We introduce a rotating coordinate system $\theta_R = \theta - \Omega t$ with $\hat{v}_\theta = v_\theta - r\Omega$ where the subscript R denotes the relative frame of reference, $\hat{v}_\theta$ denotes the relative tangential velocity and Ω is the rotational speed of the rotor. By the chain rule it follows that

$$\frac{\partial}{\partial t} \to \frac{\partial}{\partial t} - \Omega\frac{\partial}{\partial \theta} \qquad \frac{\partial}{\partial \theta} \to \frac{\partial}{\partial \theta_R}$$

Therefore, for any variable w:

$$\frac{\partial(rw)}{\partial t}+v_\theta\frac{\partial w}{\partial\theta}\to\frac{\partial(rw)}{\partial t}-\Omega r\frac{\partial w}{\partial\theta_R}+(\hat{v}_\theta+r\Omega)\frac{\partial w}{\partial\theta_R}$$
$$=\frac{\partial(rw)}{\partial t}+\hat{v}_\theta\frac{\partial w}{\partial\theta_R} \qquad (2)$$

Using the transformation (2) the equations in the rotating frame of reference are

$$\frac{\partial(r\rho)}{\partial t}+\frac{\partial(r\rho v_r)}{\partial r}+\frac{\partial(\rho\hat{v}_\theta)}{\partial\theta_R}+\frac{\partial(r\rho v_z)}{\partial z}=0$$

$$\frac{\partial(r\rho v_r)}{\partial t}+\frac{\partial\left(r\left(\rho v_r^2+p\right)\right)}{\partial r}+\frac{\partial(\rho v_r\hat{v}_\theta)}{\partial\theta_R}+\frac{\partial(r\rho v_r v_z)}{\partial z}=\rho v_\theta^2+p$$

$$\frac{\partial(r^2\rho v_\theta)}{\partial t}+\frac{\partial(r^2\rho v_\theta v_r)}{\partial r}+\frac{\partial\left(r(\rho v_\theta\hat{v}_\theta+p)\right)}{\partial\theta_R}+\frac{\partial(r^2\rho v_\theta v_z)}{\partial z}=0 \qquad (3)$$

$$\frac{\partial(r\rho v_z)}{\partial t}+\frac{\partial(r\rho v_r v_z)}{\partial r}+\frac{\partial(\rho\hat{v}_\theta v_z)}{\partial\theta_R}+\frac{\partial\left(r(\rho v_z^2+p)\right)}{\partial z}=0$$

$$\frac{\partial(r\rho E)}{\partial t}+\frac{\partial(r\rho H v_r)}{\partial r}+\frac{\partial(\rho H\hat{v}_\theta+r\Omega p)}{\partial\theta_R}+\frac{\partial(r\rho H v_z)}{\partial z}=0$$

The dependent variables are based on the nonrotating velocity components even though the independent variables are the rotating coordinates. The velocity in the rotating system, $\hat{v}_\theta$, appears in the differential terms along with the velocity in the fixed frame, v_θ. We note that the energy equation has an extra term $r\Omega p$ within the θ_R derivative. These are the equations that are used for all the results presented.

MATRIX VISCOSITY

To derive a matrix viscosity [7] we first express the Euler equations in primitive variables, $w_0=(p,v_r,v_\theta,v_z,S)$ where S is the entropy. We eliminate the total energy by the use of relation (1) to introduce an equation for the pressure instead of the total energy. We also use the relationship between the entropy, S, pressure, p and the density, ρ :

$$pdS=dp-c^2d\rho=dp-\frac{\gamma p}{\rho}d\rho$$

We stress that (1) depends on the non-rotated tangential velocity. As before, we introduce the rotating system, define $\hat{v}_\theta$ and use the chain rule. We again find that the Ω term introduced by using $\hat{v}_\theta$ instead of v_θ exactly cancels the Ω introduced by the chain rule (see (2)). The result is

$$\frac{\partial p}{\partial t}+v_r\frac{\partial p}{\partial r}+\frac{\hat{v}_\theta}{r}\frac{\partial p}{\partial\theta_R}+v_z\frac{\partial p}{\partial z}+\rho c^2\left(\frac{\partial v_r}{\partial r}+\frac{1}{r}\frac{\partial\hat{v}_\theta}{\partial\theta_R}+\frac{\partial v_z}{\partial z}\right)=-\frac{\gamma v_r p}{r}$$

$$\frac{\partial v_r}{\partial t}+v_r\frac{\partial v_r}{\partial r}+\frac{\hat{v}_\theta}{r}\frac{\partial v_r}{\partial\theta_R}+v_z\frac{\partial v_r}{\partial z}+\frac{1}{\rho}\frac{\partial p}{\partial r}=-\frac{v_\theta^2}{r}$$

$$\frac{\partial v_\theta}{\partial t}+v_r\frac{\partial v_\theta}{\partial r}+\frac{\hat{v}_\theta}{r}\frac{\partial v_\theta}{\partial\theta_R}+v_z\frac{\partial v_\theta}{\partial z}+\frac{1}{r\rho}\frac{\partial p}{\partial\theta_R}=-\frac{v_\theta v_r}{r}$$

$$\frac{\partial v_z}{\partial t}+v_r\frac{\partial v_z}{\partial r}+\frac{\hat{v}_\theta}{r}\frac{\partial v_z}{\partial\theta_R}+v_z\frac{\partial v_z}{\partial z}+\frac{1}{\rho}\frac{\partial p}{\partial z}=0 \quad (4)$$

$$\frac{\partial S}{\partial t}+v_r\frac{\partial S}{\partial r}+\frac{\hat{v}_\theta}{r}\frac{\partial S}{\partial\theta_R}+v_z\frac{\partial S}{\partial z}=0$$

or in matrix form, $w_0=(p,v_r,v_\theta,v_z,S)^t$

$$\frac{\partial w_0}{\partial t}+A\frac{\partial w_0}{\partial r}+\frac{B}{r}\frac{\partial w_0}{\partial\theta_R}+C\frac{\partial w_0}{\partial z}=R(w_0)$$

The matrices A,B,C for the primitive variables are identical to those in Cartesian coordinates except that the relative velocity component $\hat{v}_\theta$ appears rather then the absolute velocity component v_θ. In particular, the eigenvalues of the system depend on the relative velocity components.

We present the artificial viscosity in the axial direction. The total artificial viscosity is a sum of similar terms in all the coordinate directions. We consider a generalized coordinate ξ direction, $\Delta\xi=1$. Then

$$w_t+F_{i+1/2,j,k}-F_{i-1/2,j,k}=d_{i+1/2,j,k}-d_{i-1/2,j,k}$$

Let $A=\frac{\partial F}{\partial w}$ and suppressing the j,k index we get

$$d_{i+1/2}=\left(|\sigma(A)|\right)_{i+1/2}\left(\varepsilon^{(2)}\left(w_{i+1}-w_i\right)-\varepsilon^{(4)}\left(\Delta^2 w_{i+1}-\Delta^2 w_i\right)\right)$$

Δ^2 is the second difference operator. $\varepsilon^{(2)}=\nu^{(2)}F(p)$ where $F(p)$ is a function of the pressure that is close to one near shocks and small in regions away from shocks. $\varepsilon^{(4)}=\nu^{(4)}G$ where G is zero near shocks and close to 1 in smooth regions. Hence, the first difference is turned on near shocks while the third difference is turned on in smooth regions of the flow. In addition, the artificial viscosity in the boundary layer is completely eliminated, based on turbulence data, for the momentum and energy equations in smooth flow. This guarantees that the artificial viscosity will not overwhelm the physical viscosity within the boundary layer. The artificial viscosity is furthered reduced in low speed regions by

a Mach number dependent function. This prevents overshoots near the leading and trailing edges. In all the cases presented we chose $\nu^{(2)} = \frac{1}{2}$ and $\nu^{(4)} = \frac{1}{128}$.

$\sigma(A)$ is a function of the matrix A. A scalar viscosity [3] uses for σ the spectral radius of A times the identity matrix. The matrix viscosity [7] is based on the absolute value of the matrix A. If we diagonalize the matrix A then $D = TAT^{-1}$. The absolute value of A is defined as $|A| = T^{-1}|D|T$. The eigenvalues of $|D|$ can vanish near stagnation points and sonic lines. To prevent this, we cutoff these values at a percentage of the spectral radius of $|D|$. In one space dimension this would give for the diagonal elements, d_i of $|D|$

$$d_0 = max(|u|, V_l(|u| + c)) \quad d_\pm = max(|u \pm c|, V_n(|u| + c))$$

where u is the velocity and c is the speed of sound. When $V_n = V_l = 1.0$ we recover the scalar artificial viscosity. Typical values are $V_n = 0.3$, $V_l = 0.1$. T depends on the absolute velocity components while the diagonal elements of D (eigenvalues) depend on the relative velocity components. Thus, the matrix artificial viscosity is similar to that given in [7]. The difference is that the eigenvalues are based on relative velocities and the matrix $|B|$ contains a $\frac{1}{r}$ term. In primitive variables, w_0, we have

$$|B_0| = \begin{pmatrix} \frac{|\hat{v}_\theta + c| + |\hat{v}_\theta - c|}{2} & \rho c \frac{|\hat{v}_\theta + c| - |\hat{v}_\theta - c|}{2} & 0 & 0 \\ \frac{|\hat{v}_\theta + c| - |\hat{v}_\theta - c|}{2\rho c} & \frac{|\hat{v}_\theta + c| + |\hat{v}_\theta - c|}{2} & 0 & 0 \\ 0 & 0 & |\hat{v}_\theta| & 0 & 0 \\ 0 & 0 & 0 & |\hat{v}_\theta| & 0 \\ 0 & 0 & 0 & 0 & |\hat{v}_\theta| \end{pmatrix}$$

where c is the speed of sound. Rewriting the above in conservative variables, $w_c = (\rho, \rho v_r, \rho v_\theta, \rho v_z, E)$, we use $\frac{\partial w_c}{\partial w_0}|B_0|\frac{\partial w_0}{\partial w_c}$. $|B_0|$ depends on the relative velocity components while the Jacobians $\frac{\partial w_c}{\partial w_0}, \frac{\partial w_0}{\partial w_c}$ depend on the absolute velocity components.

The rationale for matrix viscosity is that it adds different amounts of artificial viscosity to each wave. The scalar viscosity adds dissipation proportional to $q + c$ to all waves. However, the matrix viscosity adds dissipation proportional to q to the entropy and vorticity waves. Hence, one expects less diffusion of the vorticity and entropy waves with the matrix valued viscosity compared with the scalar viscosity.

PRECONDITIONING

It is known that when the Mach number becomes small that the convergence to a steady state of standard compressible codes becomes very slow. This occurs because of the stiffness in the equations caused by the large ratio of the acoustic to convective speed. The purpose of the preconditioner is to change the speeds of the waves so that the ratio of the various speeds remains finite as the Mach number approaches zero. We consider preconditioning for the system in the rotating coordinate system (3) or equivalently (4). The fluid dynamic equations are replaced by

$$P^{-1}w_t + f_z + g_r + h_\theta = R$$

We consider low speed preconditionings based on the homogenous Euler equations in the rotating coordinate system given by (4). This preconditioning is the same as presented in [8; 9; 12] except that β now depends on the relative velocity

$$P = \text{diag}(\beta^2, 1, 1, 1, 1)$$

In addition to a slowing of the convergence the accuracy of the resultant numerical system deteriorates as the Mach number becomes small. This is caused by an improper scaling of the standard artificial viscosity or upwinding as the Mach number approaches zero. So, the preconditioner improves both the acceleration to a steady state and simultaneously improves the accuracy of the numerical solution at the steady state as the Mach number approaches zero [10; 12].

We shall only consider preconditioning coupled with a scalar viscosity. One could also use a matrix viscosity that depends on the preconditioning [12]. Since the preconditioning only equalizes wave speeds, it does not include effects of the lower order terms. Thus, the preconditioning in Cartesian coordinates and cylindrical coordinates is the same (accounting for the $\frac{1}{r}$ in the θ_R direction). With the rotating coordinate system it is the rotated velocity components that appear in the preconditioning matrix for the primitive variables (p, u, v, w, S). Similarly for (p, u, v, w, T) variables, where T is the temperature, since the transformation from S to T depends only on thermodynamic quantities. If the preconditioning matrix is written in conservation variables then both relative and absolute velocities appear because the transformation from (p, u, v, w, S) variables to conservative variables depends on the absolute velocity components.

When $\beta = 1$ we revert to the standard equations. For the ratio of the eigenvalues to become finite at $M = 0$ we require that $\beta \sim M_{\text{rel}}$ where M_{rel} is the relative Mach number.. This become singular at $M_{\text{rel}} = 0$ which arises when the Mach number locally approaches zero near the stagnation point. Hence, it is necessary to prevent β from becoming too small. This rationale indicates that we can cutoff β at some very low level. Turkel has suggested the following cutoff [8]

$$\beta^2 = \min\left(\max(K_1 M_{\text{rel}}^2, \beta_{min}^2), 1\right) \quad \beta_{min}^2 = K_2 M_{ref}^2 \quad K_1 = 1.1$$

For external flow one usually chooses M_{ref} based on the Mach number at infinity. For turbomachinery the inflow is usually not

constant and so it does not provide a good basis for a lower bound. Instead, we choose M_{ref} equal to the largest value of the relative Mach number in the initial flow. K_2 seems to be problem dependent which is still the main drawback to the robustness of these methods. In most cases we choose $K_2 = 1$. This implies that β is almost constant (β_{min}) for much of the region.

In low Mach number flows, the flow is almost incompressible and the density is almost constant. Hence, conservative variables, w_c, are not the best choice. Instead we evaluate the artificial viscosity and update the solution using $(p, v_r, v_\theta, v_z, T)$ variables. All physical fluxes are based on conservative variables.

RESULTS

Matrix viscosity and preconditioning are tested on a transonic rotor. The preconditioner is tested on selected blade rows of a multistage compressor. Both machines have experimental data available. Comparisons to data are made where possible.

ROTOR 35

To demonstrate the advantages of these improvements to the code for a three dimensional case we consider a transonic rotor that was designed, built and tested at NASA Glenn Research Center [15; 16]. This geometry is called Rotor 35. The rotor has 36 blades spinning at $13,751 RPM$ which corresponds to 80% of design speed. The aspect ratio is 1.19 and radius ratio is 0.70. The tip clearance gap is $0.74 mm$ and is the distance between the rotor tip and the shroud at the design condition. Overall performance data from aerodynamic probe surveys were taken at Station 1 and Station 4 which are indicated in Figure 1.

The mesh used to simulate Rotor 35 contained a total of $851,400$ cells. In the axial direction, 70 cells are distributed along the blade chord, 50 cells are distributed in the pitch-wise direction and 86 cells are distributed from hub to the casing. The last 12 cells from the casing are placed within the clearance gap and model the clearance flow. We compare the results of the simulations with data taken by Van Zante, et al. [15]. The experiment had a small amount of flow leakage from the gap between the stationary and rotating part of the hub upstream of the rotor. The small amount of leakage was included in the simulations. The operating point for the simulations is near the peak efficiency condition. This was obtained by setting the static pressure at the hub of Station 4. Station 4 is where the global computational grid is terminated and is about one chord downstream of the blade.

We compare the original non-preconditioned scalar viscosity, the matrix viscosity and preconditioning with a scalar viscosity. The purpose of each of these improvements are different. The matrix viscosity is designed to reduce the total artificial viscosity and so improve the accuracy of the numerical solution. We compare the matrix viscosity with $V_n = .3$ and $V_l = 0.1$ to the scalar artificial viscosity. Figure 2 is a plot of the pressure ratio

versus mass flow of both simulations compared to the experimental data. The pressure ratio is defined as the mass-averaged total pressure of the flow at station 4 normalized by the total pressure at station 1. The open symbols evaluate the pressure ratio using all the available mesh points. The solid symbols evaluate the pressure ratio using only the radial locations at which the experimental data was obtained. The pressure ratio of both simulations underpredict the experiment. Note that the pressure ratio computed using the radial locations at which the data was obtained moves the pressure ratio toward the data. There is virtually no difference in pressure ratio using the matrix viscosity or the scalar viscosity. Both set of results are within 1.5% of the measured pressure rise across the rotor. Figure 3 is a plot of the computed efficiency versus mass flow compared to the experimental data. The efficiency is the ratio of ideal work input to actual work input. The matrix viscosity shows an increase in efficiency of .2% using all available mesh points over the scalar viscosity. The increase in efficiency using the experimental reporting locations is .1%.

Figure 4 is a plot of the mass-averaged total pressure ratio versus percent span for the scalar and matrix viscosity simulations compared to the experimental data. There is very little difference between the simulations. However, figure 5 compares the efficiency profiles and shows a fuller profile for the matrix viscosity simulation in the lower span region Looking more closely at the three dimensional flow field one finds that the matrix viscosity decreases the size of the boundary layer and so decreases the effective blockage in the rotor.

We next consider the same case using preconditioning and a scalar viscosity. Because of the transonic flow we do not expect to see much of a difference in the solution. Figure 6 shows virtually no difference in the total pressure profile from the scalar viscosity solution. There is also little difference in the convergence rate using the preconditioner.

LSAC

To test the effectiveness of the preconditioner on low-speed flows, the Inlet Guide Vane (IGV) and first rotor of the Glenn Low Speed Axial Compressor (LSAC) were simulated as isolated blade rows. LSAC is a four and a half stage machine, [16] which is representative of the rear stages of a high pressure compressor. The simulation of the rotor accounted for tip clearance but did not include casing treatment over the first rotor which is present in the experiment. Figure 7 is a drawing of the LSAC. The IGV is between Stations 0.5 and 1.0 and the first rotor is between Stations 1.0 and Stations 1.5. The inlet and exit locations of the computational domain were placed a chord length upstream and downstream of the blade row under consideration.

Both the IGV and first rotor were simulated near the peak efficiency operating point. The inlet conditions of each blade row: total pressure; total temperature; and flow angle were obtained

from a data match of the experimental data. The exit conditions were also obtained from this data match of the experimental data. Inflow Mach numbers can go down to 0.05 in these simulations and so we expect preconditioning to help both the convergence to a steady state and accuracy of the steady state approximation.

In figure 8 the convergence rate for the IGV is plotted with and without preconditioning. We see that the case without pre-conditioning converged after 6000 iterations while the case with preconditioning converged after about 1200 iterations. Hence, the preconditioning leads to a factor of five improvement in the number of iterations required for convergence. These simulations were run on an SGI Origin 200 using $270Mhz$ processors. The preconditioner on this processor requires an additional 40% of CPU time compared to without preconditioning. Factoring this into the iteration count, the preconditioning yields nearly a four-fold speedup. This is shown in figure 9 where the normalized iteration for the preconditioner is multiplied by a factor of 1.40, in effect, changing the comparison of the two cases to a normalized CPU time.

In figure 10 we plot the total pressure coefficient as a function of span for the two cases with the experimental data at the exit of the IGV. The total pressure coefficient is defined as the total pressure normalized by the inlet dynamic pressure. The simulation results are averaged in the pitch-wise direction. Both profiles follow the experimental data for most of the span. Note that the profile resulting from preconditioning follows the data near the hub region closer than without preconditioning.

We next consider the first rotor of LSAC. The convergence rate for the preconditioned case and non-preconditioner case is plotted in figure 11 in terms of the total pressure coefficient at the exit. Figure 12 is a plot of the convergence rate in terms of inlet mass flow. In this case, the results are converged within 2500 iterations with preconditioning but are quite oscillatory even after 7000 iterations without preconditioning. To include the additional overhead of applying the preconditioner, we multiply the preconditioner iteration count by a factor of 1.4. This results in convergence of the preconditioner in 3500 normalized iterations. This is shown in figure 13 for the massflow convergence. In figure 14 we display the pitch-wise, mass-averaged total pressure coefficient at rotor exit while in figure 15 we present the absolute flow angle at rotor exit. We again compare the results with and without preconditioning to the experimental data. Now, the total pressure coefficient profile from both simulations show similar profiles. They both overpredict the hub and casing region. The first rotor has casing grooves and leakage flow in the gap between the rotating and stationary parts of the hub geometry. These were not modeled and, at the high flow condition that was simulated, the effect of these should be minimal. It is not clear what is causing these differences.

CONCLUSION

A matrix viscosity and low Mach number preconditioner have been implemented into an existing flow solver used to simulate the flow through turbomachinery. The matrix viscosity is designed to reduce the artificial viscosity level. The matrix viscosity was tested on a transonic rotor and showed an improvement in the efficiency of the machine relative to available experimental data. The preconditioner was tested on an IGV and rotor of a low Mach number compressor and showed a sizable increase in convergence rate in both simulations. The results of these tests on isolated blade row geometries suggest these improvements be further studied on multistage turbomachine geometriess.
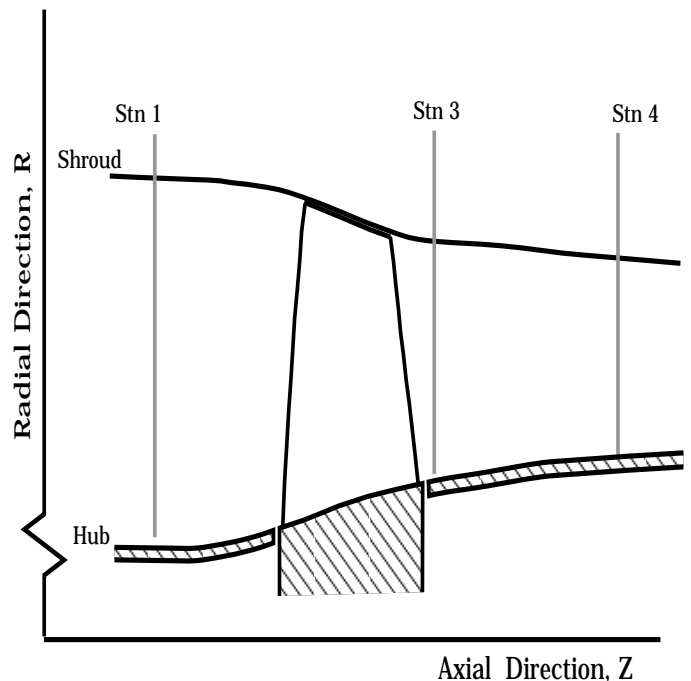
Acknowledgment

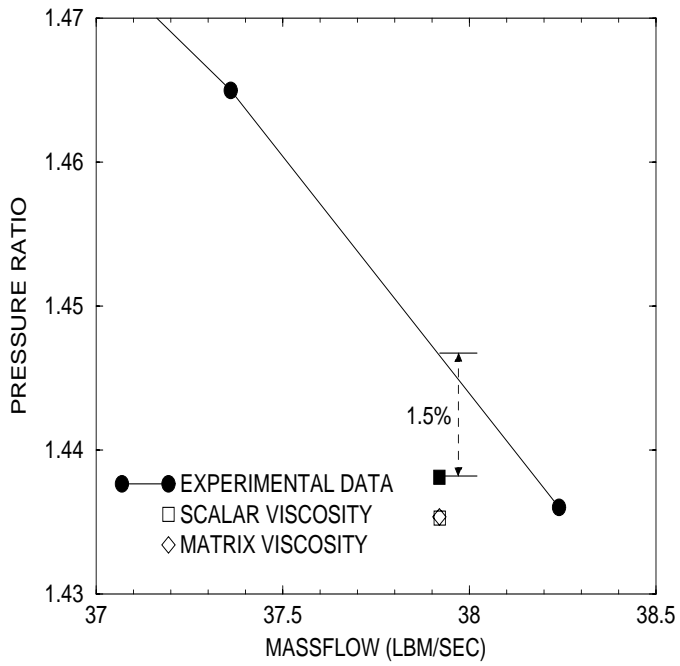Figure 1. Rotor 35 flowpath indicating locations of Stations 1, 3 & 4.

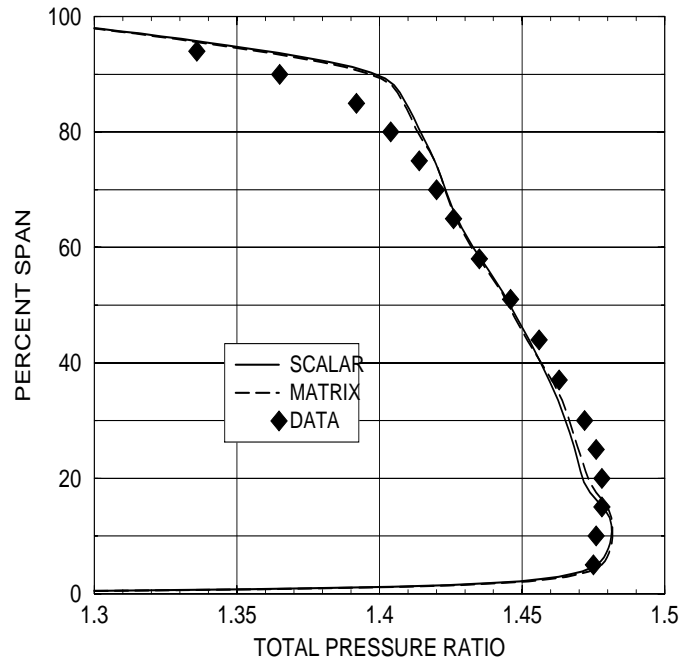Figure 2. Comparison of Pressure Ratio with the Experimental Speed-line of Rotor 35 at 80% speed.

Figure 4. Comparison of Total Pressure Profiles with Experimental Data.
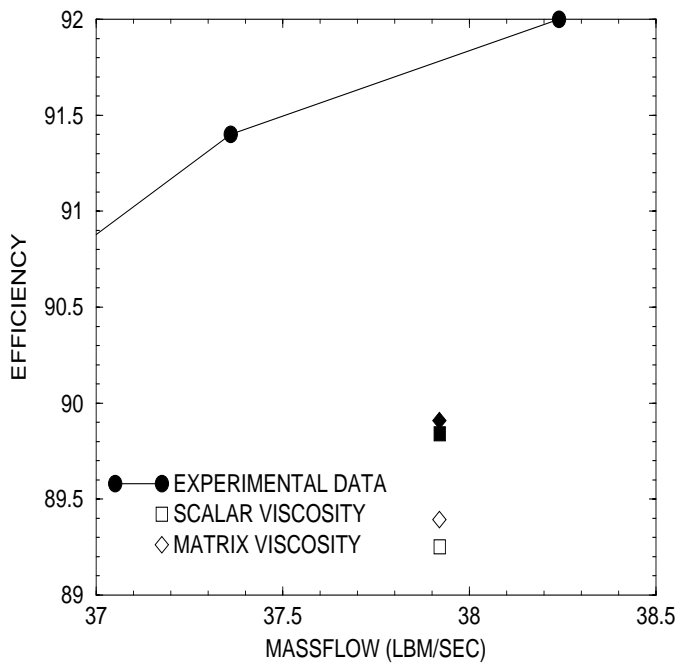

Figure 3. Comparison of Efficiency with the Experimental Speedline of Rotor 35 at 80% speed.
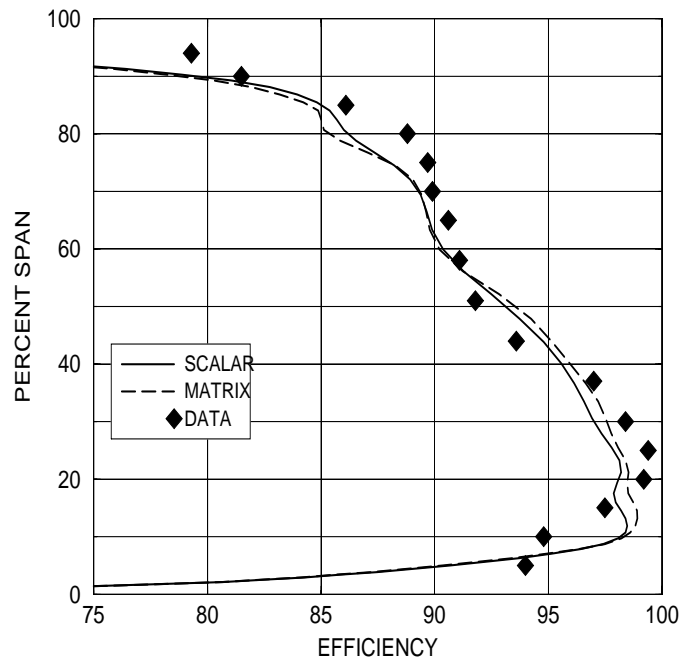

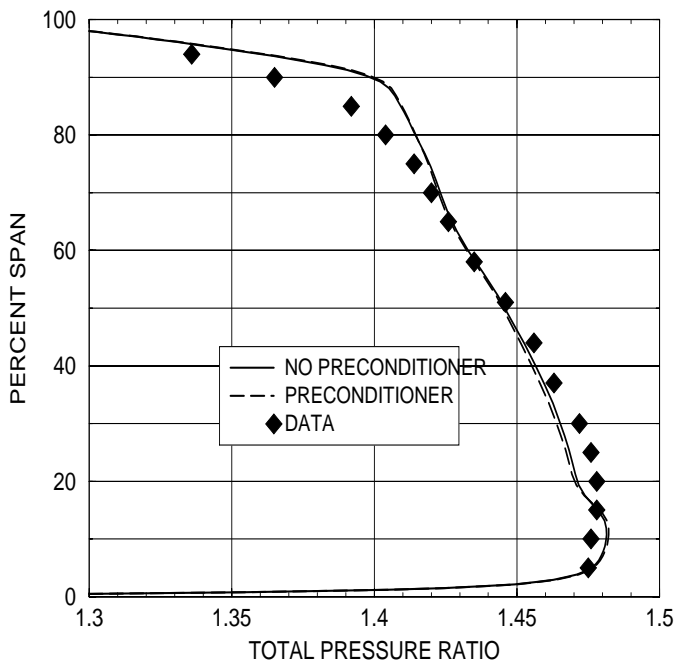Figure 5. Comparison of Efficiency Profiles with Experimental Data.

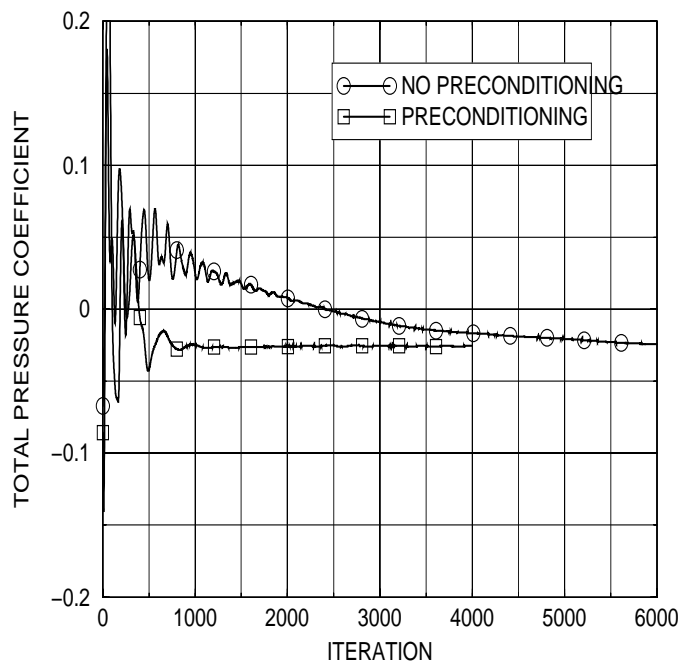Figure 6.   Comparison of Total Pressure Profiles with Experimental Data.

Figure 8.   Convergence Rate of Total Pressure Coefficient with Preconditioning for IGV.
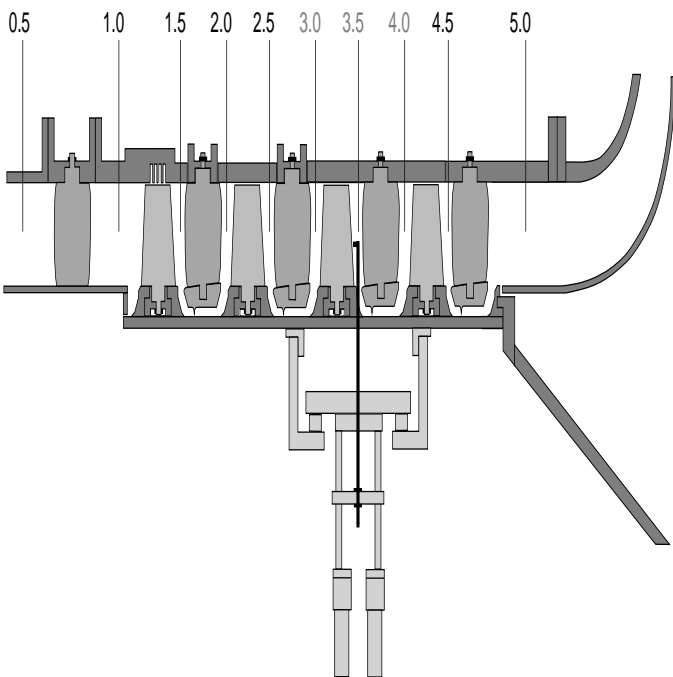
Figure 7.   Sketch of Low-Speed Axial Compressor (LSAC).
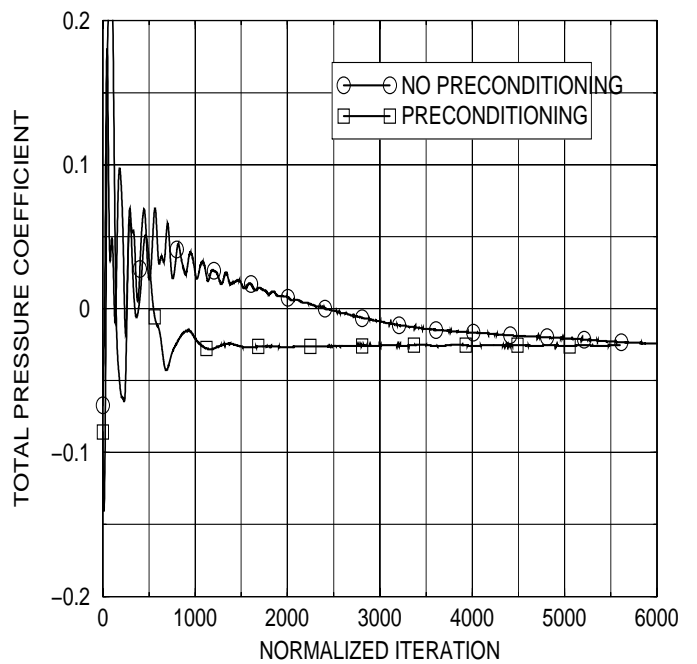
Figure 9.   Normalized Convergence Rate for previous case

7
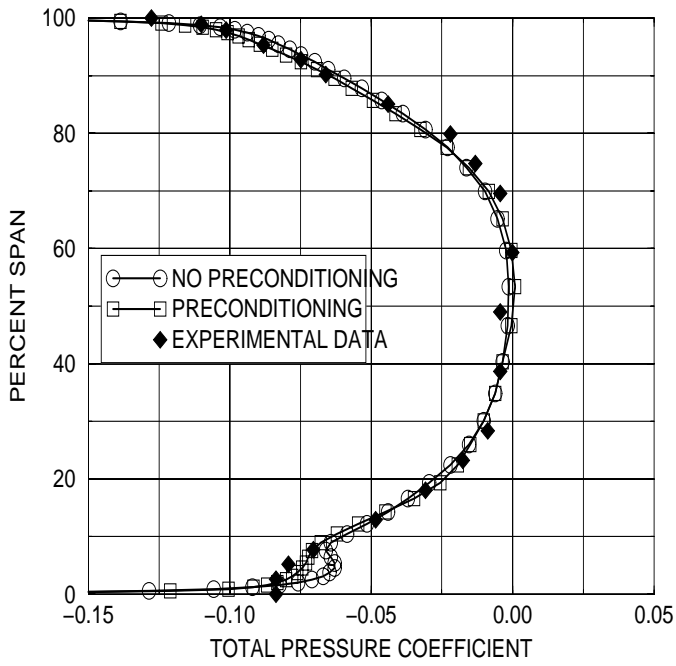
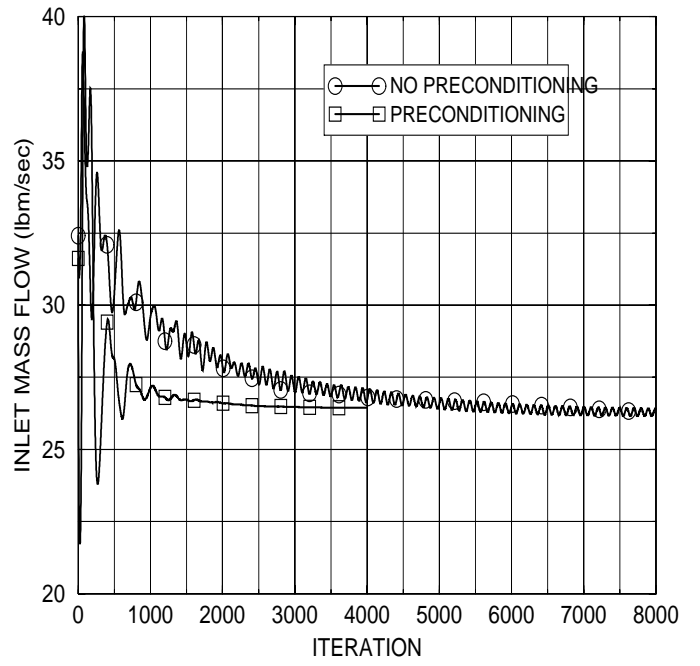Figure 10.   Profile of Total Pressure Coefficient at Exit for LSAC IGV.

Figure 12.   Convergence rate for Mass Flow in LSAC Rotor 1.
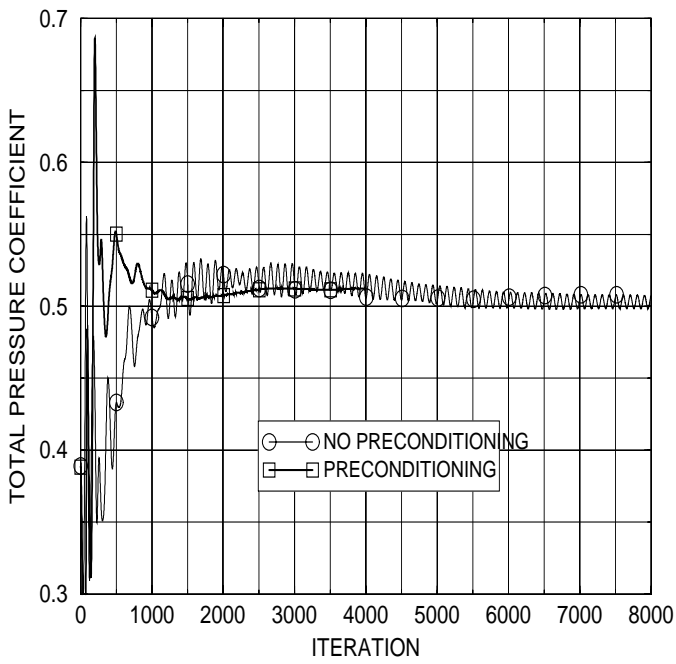

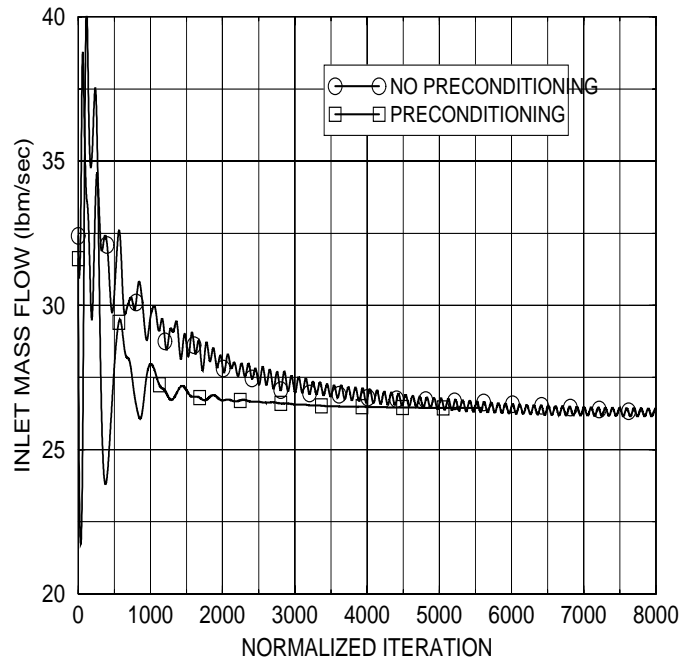Figure 11.   Convergence rate for Total Pressure Coefficient in LSAC Rotor 1.

Figure 13.   Normalized Convergence rate for Mass Flow in LSAC Rotor 1.
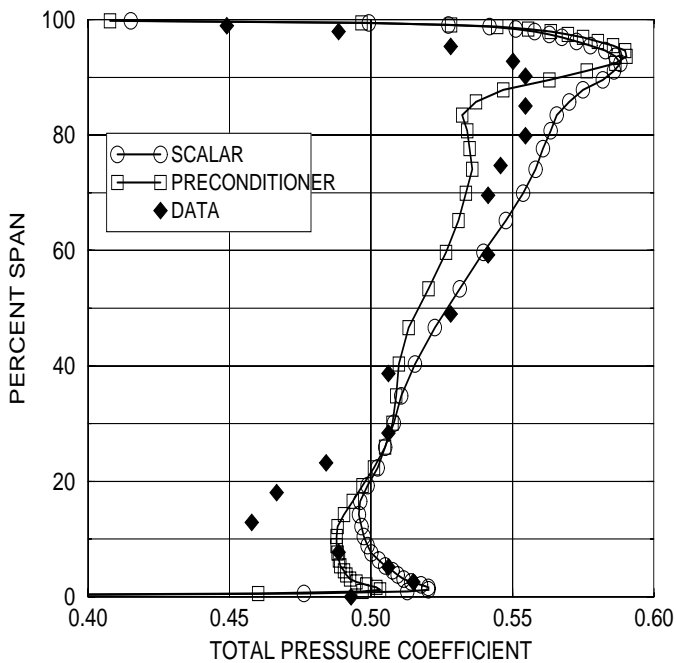
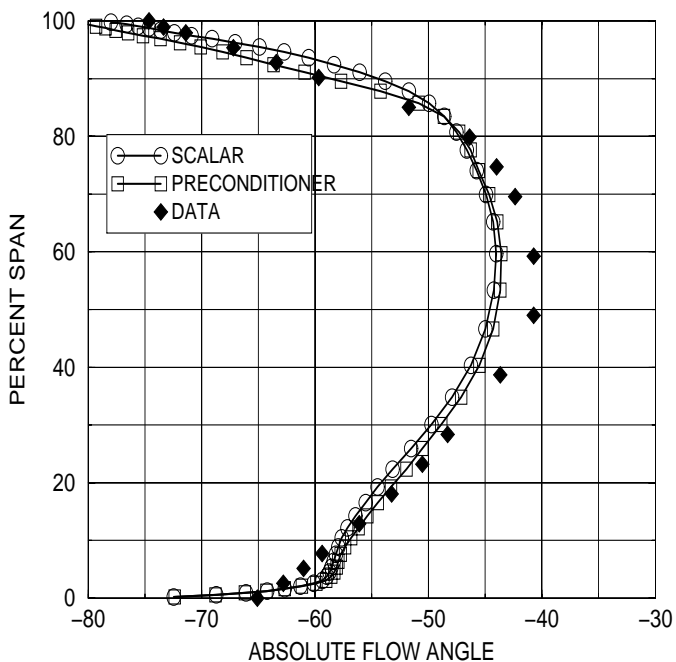Figure 14.   Total Pressure Coefficient in LSAC rotor

Figure 15.   Absolute Flow Angle in LSAC rotor

REFERENCES

J.J. Adamczyk, M.L. Celestina, T.A. Beach and M. Barnett, Simulation of Three-Dimensional Viscous Flow Within a Multistage Turbine, AMSE 89-GT-152 (1989).

M.L. Celestina, R.A. Mulac and J.J. Adamczyk, A Numerical Simulation of the Inviscid Flow Through a Counterrotating Propellor, AMSE paper 86-GT-138 (1986).

A. Jameson, W. Schmidt and E. Turkel, Numerical Solutions of the Euler Equations by Finite Volume Methods Using Runge-Kutta Time-Stepping Schemes, AIAA Paper 8l-l259 (198l).

K.R. Kirtley, T.A. Beach and J.J. Adamczyk, Numerical Analysis of Secondary Flow in a Two-Stage Turbine, AIAA Paper 90-2356 (1990).

A. Shabbir, M.L. Celestina, J.J. Adamczyk and A.J. Strazisar, The Effect of Hub Leakage Flow on Two High-Speed Axial Flow Compressor Rotors, ASME Paper 97-GT-346 (1997).

K.L. Suder and M.L. Celestina, Experimental and Computational Investigation of the Tip Clearance Flow in a Transonic Axial Compressor Rotor, ASME paper 94-GT-365 (1994).

R.C. Swanson and E. Turkel, On Central Difference and Upwind Schemes, *J. Comput. Phys.* 101:292-306 (1992).

E. Turkel, Preconditioned Methods for Solving the Incompressible and Low Speed Compressible Equations, *J. Comput. Phys.* 72:277-298 (1987).

E. Turkel, A Review of Preconditioning Methods for Fluid Dynamics, *Applied Numerical Mathematics*, 12:257-284 (1993).

E. Turkel, A. Fiterman and B. van Leer, Preconditioning and the Limit of the Compressible to the Incompressible Flow Equations for Finite Difference Schemes, *Frontiers of Computational Fluid Dynamics 1994*, 215-234. D.A. Caughey and M.M. Hafez editors, John Wiley and Sons (1994).

E. Turkel, R. Radespiel and N. Kroll, Assessment of Two Preconditioning Methods for Aerodynamic Problems, *Computers and Fluids* 26:613-634 (1997).

E. Turkel, Preconditioning Techniques in Computational Fluid Dynamics, *Annual Review of Fluid Mechanics 1999, 385-416* (1999).

E. Turkel, Robust Preconditioning for Steady and Unsteady Viscous Flows, AIAA paper 2002-0962 (2002).

D.L. Tweedt, R.V. Chima and E. Turkel E, Preconditioning for Numerical Simulation of Low Mach Number Three-Dimensional Viscous Turbomachinery Flows, AIAA paper 97-1828 (1997).

Van Zante, Strazisar, Wood, Hathaway and Okiishi, Recommendations for Achieving Accurate Numerical Simulation of Tip Clearance Flows in Transonic Compressor Rotors, J. of Turbomachinery, V. 122, Oct. 2000.

S.R. Wellborn and T.H. Okiishi, Effects of Shrouded Stator Cavity Flows on Multistage Compressor Aerodynamic Performance, NASA CR 198536 (1996).